Translational Oncology 56 (2025) 102388

Contents lists available at ScienceDirect

Translational Oncology

journal homepage: www.elsevier.com/locate/tranon

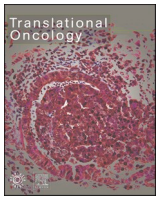

Original Research

Characterization of a novel cell line established from mice gastrointestinal stromal model by chemical induction

Zhan Zhao [a,1], Shenghui Qiu [a,b,1], Xiangwei Zhang [a,1], Shijin Liu [a], Lu Wang [c], Hanyang Guan [a], Jiashuai He [a], Yangzhi Hu [d], Xiaobo Li [e], Simin Luo [f], Zuyang Chen [a], Tianmu Mo [a], Yiran Zhang [a], Xiaoxu Zhao [a], Yunlong Pan [a], Hui Ding [a,*], Jie Cao [a,b,*], Jinghua Pan [a,*]

[a] Department of General Surgery, The First Affiliated Hospital of Jinan University, 510632, Guangzhou, Guangdong, PR China
[b] Department of General Surgery, Guangzhou First People's Hospital, Guangzhou, 510180, PR China
[c] Institute of Precision Cancer Medicine and Pathology, Jinan University Medical College, Guangzhou, Guangdong, 510632, PR China
[d] The Affiliated Hospital of Xiangnan University, Chenzhou, Hunan, PR China
[e] State Key Laboratory of Bioactive Molecules and Druggability Assessment, Jinan University, Guangzhou, 510632, China
[f] Department of Bone and Joint Surgery, The First Affiliated Hospital, Jinan University, Guangzhou, Guangdong Province, China

ARTICLE INFO

Keywords:
Gastrointestinal stromal tumors (GIST)
mGSTc01
Mouse cell line
C57BL/6 J
C-kit

ABSTRACT

Background: Gastrointestinal stromal tumors (GISTs) are a type of tumor that originates from gastrointestinal mesenchymal tissue. Although several somatic or germline mutation GIST mice were established, however, there is still a lack of an authentic mice GIST cell lines for further experimental study.
Methods: We developed a chemically induced C57BL/6 J GIST model using 3- methylcholanthrene. Tumor characteristics were confirmed through histology and IHC. Primary cells were isolated to establish the mGSTc01 cell line, and molecular profiling was conducted. Additionally, we established GIST model in immunocompetent mice to evaluate their sensitivity to imatinib.
Results: Our study successfully developed a chemically induced murine GIST model, characterized by positive staining of c-kit and DOG-1. The mGSTc01 monoclonal cell line exhibited slender morphology and expressed the c-kit marker, Whole exome sequencing uncovered mutations of Lamb1, MMP9, and c-kit in GIST cells and provided a detailed picture of the entire genome's copy number variations. RNA sequencing indicated genes associated with cell adhesion and focal adhesion were enriched in mGSTc01 cells. The mGSTc01 cells demonstrated obvious malignant behaviors, notably elevated migration, adhesion, and proliferation. In immunocompetent mice, subcutaneous xenografts not only reserved the aggressive phenotype but also displayed a response to imatinib, underscoring the model's applicability for advancing therapeutic research.
Conclusion: We firstly established a mGSTc01 cell line derived from C57BL/6 J mice GIST tumor offers, which closely mimicking human disease characteristics. It is a potent platform for investigating tumor microenvironment of GIST in mice model, and provides a novel way for new therapeutic discoveries in GIST.

Background

Mesenchymal gastrointestinal cancers, such as gastrointestinal stromal tumors (GISTs), are found throughout the entire gastrointestinal tract [1]. Globally, the annual incidence of GIST is estimated at 10–15 cases per million individuals [2]. Notably, the prevalence of GIST in east Asia significantly exceeds that observed in North America [2,3]. GIST are predominantly located in the stomach, accounting for approximately 60 % of cases, followed by the small intestine with about 30 % of occurrences. Additionally, GISTs also can be detected in the duodenum (comprising 4–5 % of cases), rectum (2–4 %), colon (1–2 %), and, less commonly, in the esophagus (below 1 %) [4–6]. GISTs are acknowledged to derived from the interstitial cells of Cajal (ICCs), which act as pacemaker cells within the gastrointestinal wall. Cajal are part of the larger group of cells known as the stromal cells of the muscularis propria. The abnormal proliferation of ICCs leads to the formation of

* Corresponding authors at: Department of General Surgery, The First Affiliated Hospital of Jinan University, Guangzhou, Guangdong, 510632, PR China.
E-mail addresses: 6432206@163.com (H. Ding), eycaojie@scut.edu.cn (J. Cao), panjh@jnu.edu.cn (J. Pan).
[1] These authors contributed equally to this manuscript.

https://doi.org/10.1016/j.tranon.2025.102388
Received 23 September 2024; Received in revised form 3 February 2025; Accepted 5 April 2025

GISTs. Unlike epithelial cancers, which are more common and originate from the glandular cells lining the gastrointestinal tract, GISTs are derived from supportive tissues and characterized by mesenchymal phenotype [7].

GIST are predominantly driven by critical targets, such as KIT and Platelet-Derived Growth Factor Receptor Alpha (PDGFRA), both of which are tyrosine kinases, and mutations in them lead to the constitutive activation of downstream signaling axis in a ligand-independent manner, thereby facilitating the initiation and progression of GIST [8,9]. Imatinib is the standard first-line therapy for advanced GIST, improving progression-free survival. However, an increasing evidence show that tumor microenvironment (TME) is critical for tumor growth and drug resistance in GIST [10,11]. To explore the nosogenesis and mechanism of GIST, mouse-derived cell line models are important tools for studying the TME of GIST. Existing studies on GIST have primarily utilized models such as $Kit^{V558\Delta}/+$ Mice [12] or patient-derived xenografts (PDX) models [13,14], or mouse GIST cell line, S2 cell line [15]. However, the reproductive cycle for genetically engineered mice is lengthy, and the process is both costly and technically challenging [12]. Additionally, tumor cells obtained through repeated passaging and selection, similar to the S2 cell line, often have low purity and may be contaminated with other stromal cells from the tumor microenvironment [16]. Therefore, there is an urgent need to develop an innovative mouse GIST model and cell line that shortens the research cycle and offers superior cost-effectiveness.

Here, we constructed a mouse model of GIST using chemical induction methods and successfully isolated and cultured a new mouse-derived GIST monoclonal cell line, named the mGSTc01. We also identified it through various methods, including transcriptomics, whole exome sequencing (WES), and immunofluorescence. Furthermore, we successfully established a subcutaneous xenograft model of GIST using immunocompetent mice, beneficial for advancing future research on TME of GIST.

Method

Cell line and cell culture

Cajal cell were purchased from ELGBIO (Guangzhou, China). Cajal cells were grown in a specific medium (ELGBIO, Guangzhou, China) containing 10 % fetal bovine serum (FBS; FSP500, ExCell Bio, Shanghai, China) and 1 % penicillin-streptomycin (15,140,122, Gibco) and kept at 37 °C in a humidified atmosphere with 5 % CO2. All cells tested negative for mycoplasma.

Animals experiment

Female C57BL/6 J mice (4–5 weeks, weight 18 - 20 g) were obtained from BesTest Bio-Tech Co., Ltd. (Zhuhai, China). All animals were housed in ventilated cages in a temperature and light controlled room in a SPF facility. All animal experiments were approved by the Experimental Animal Ethics Committee of Jinan University. During the experimentation, mGSTc01 cells (5×10^6 cells/ml) suspended in PBS (100 μL/mice) were subcutaneous injected in female C57BL/6 J mice. When tumors grew to approximately 100 mm^3, the tumor-bearing mice were randomly divided into the saline or Imatinib group ($n = 5$). The tumor volumes were examined and calculated using the formula: Tumor volume $= 1/2 \times a \times b^2$, where a refers to the longer diameter and b indicates the shorter diameter perpendicular to a. Mice were administered with 10 mg/kg Imatinib via intraperitoneal injection every three days. After treatment for 21 days, mice were euthanized, and tumor tissues were resected, weighed, and photographed.

Isolation of gastrointestinal stromal tumor cells from mouse-derived tumor

We first constructed a mouse model of GIST. After saturating standard surgical sutures with 5 mg of 3-methylcholanthrene (3-MCA), the sutures were implanted between the muscularis propria and serosa layers at the gastric greater curvature of C57BL/6 J mice, followed by routine postoperative care and weekly abdominal palpation starting at week 12 to monitor tumor development. Then, the mouses were dissected, and the tumors were harvested. Subsequently, the adipose tissue, blood vessels, and necrotic portions were removed. Prior to enzymatic digestion, the tissue was moved to a 6-well plate and cut into small pieces of 1–2 mm3. The tissue fragments were subsequently mixed with DMEM + 100 IU/mL Penicillin and 100 μg/mL Streptomycin (1 % P/S; Gibco, Paisley, GB and Grand Island, NY, USA) and promptly transferred to a MACS C-tube containing mouse tumor dissociation enzymes, following the guidelines provided by the manufacturer (Tumor Dissociation Kit, Mouse). The process of tumor dissociation was carried out using the gentleMACSTM Octo Dissociator with tumor, using a specific cancer dissociation program, and maintaining a steady rotation at 37 °C for a duration of 1 hour. Next, the cell suspension was passed through a MACS SmartStrainer with a pore size of 70 μm. The items acquired from Miltenyi Biotec (Bergisch Gladbach, Germany) include a kit, C-Tube, strainer, devices, and programs. The strainer surface was meticulously cleared of any leftover tissue residues by gently rubbing them through the membrane using the coarse side of a 5 mL syringe punch. The strainer was then rinsed with PBS. The cells were collected and centrifuged. Tumor cells were finally cultured with RBMI medium (Gibco, Australia) in a 37 °C incubator.

Hematoxylin-eosin, immunohistochemical and cell immunofluorescence analyses

Tumors and normal stomach tissue from each animal were fixed, embedded in paraffin, cut into 4-μm slices, and subjected to hematoxylin-eosin (H&E) staining using conventional techniques. For immunohistochemical staining (IHC), the sections were deparaffinized, rehydrated, antigen retrieved by boiling with sodium citrate antigenic repair solution (pH 9.0), and blocked with 3 % BSA solution. This was followed by incubation with primary antibodies overnight at 4 °C. The slides were then incubated with horseradish peroxidase (HRP)-conjugated secondary antibodies and visualized using a DAB kit (Cat. G1212, Servicebio, Wuhan, China). Images were analyzed using an Olympus BX53 inverted epifluorescence microscope (Olympus, Japan). For cell immunofluorescence staining, the cells were seeded on confocal Petri dishes, fixed with 4 % paraformaldehyde for 20 min, and permeabilized in 0.2 % TritonX-100 for 5 min. The confocal Petri dishes were then subjected to blocking and staining, and examined using a Zeiss LSM 800 confocal microscope. Positive cells were counted at 400-fold magnification. The primary antibodies were list in the Table 1.

Table 1
Primary antibodies.

Antibody	Company
Desmin	Cell Signaling Technology
c-kit	Affinity
Dog-1	Affinity
Vimentin	Servicebio
S-100A1	Abways
SDHB	Boster
α-SMA	Servicebio
Ki67	Servicebio
APC c-kit	Biolegend
MMP2	Servicebio
CD44	Cell Signaling Technology
CHI3L1	Beyotime
COL1A2	Abcam
COL3A1	Beyotime
Col4a2	Abcam
β-actin	Servicebio
HRP- Goat Anti-Rabbit IgG ($H + L$)	Servicebio
HRP -Goat Anti-Mouse IgG ($H + L$)	Servicebio

Western blotting

To extract total protein, mGSTc01 and Cajal cells were rinsed twice with PBS (HyClone) and then lysed in ice-cold RIPA lysis buffer containing phosphatase inhibitor (Roche, Indianapolis, IN, USA) and protease inhibitor cocktail (Roche). The lysis process took place on ice for 30 min. Following centrifugation at a speed of 12,000 times the force of gravity at a temperature of 4 °C for a duration of 15 min, the liquid portion above the sediment was collected and subjected to analysis using a BCA Protein Assay Kit (Pierce, Rochford, IL, USA). Subsequently, electrophoresis and immunoblot analysis were conducted following the established protocol. The proteins and pre-stained protein marker (M221, GenStar, Beijing, China) were separated using sodium dodecyl sulfate-polyacrylamide gel electrophoresis (SDS-PAGE) gels and then transferred onto polyvinylidene fluoride membranes (Millipore). Following the blocking step, the membranes were subjected to incubation with primary antibodies, followed by incubation with anti-rabbit IgG and anti-mouse IgG. The primary antibodies were list in the Table 1

Wound-healing assays

Cells were first placed in 12-well plates at the beginning of the experiment. Once the cells attained about 80 % confluence, scratches were made in the cell monolayer using sterile 200μl pipette tips. Afterwards, these processed cells were cultured for an additional 12 h and 24 h on a medium without serum. An Olympus Corporation inverted microscope from Japan was used to study the healing process of cell damage. Ultimately, the wound area was analyzed quantitatively using ImageJ software to evaluate the extent of cell migration and the capacity for healing.

Cell adhesion assay

To assess cell adhesion ability, 96-well plates were coated in advance with a concentration of 50 μg/mL of human fibronectin (Corning, MA, USA) and left overnight at a temperature of 4 °C. Next, the mGSTc01 and Cajal cells were collected, and 5000 cells were suspended in 100 μL of RBMI without serum. These cells were then placed in the 96-well plates that had been previously coated. The nonadherent cells were eliminated after being incubated at a temperature of 37 °C for 4 h and 8 h. The cells that were attached were rinsed two times with PBS, treated with 4 % paraformaldehyde to preserve their structure, and then colored with 0.1 % crystal violet. The quantity of cells attached to the fibronectin was measured using an inverted microscope.

Cell proliferation assay

The mGSTc01 and Cajal cell (5×10^3) were cultured in 96-well plates for 48 h after which cell proliferation was assessed using the Beyo-Click™ EdU Cell Proliferation kit (Cat. C0071S, Beyotime, Shanghai, China) and analyzed with Image Pro Plus 6 software.

Cell migration assay

The distinction between mGSTc01 cell and Cajal cell migration were determined by a Transwell assay. In summary, mGSTc01 cell and Cajal cell (2×10^4 cells/well) were placed in 100 μL of serum-free DMEM and added to the top chambers of a Transwell plate (24-well plate, 8-mm pore size, Corning). Subsequently, 500 microliters of DMEM solution containing 10 % FBS was introduced into the bottom chambers. Following a 24-hour period of cultivating, the cells were treated with 4 % paraformaldehyde at room temperature for 30 min to fix them. Subsequently, the cells were stained with 0.1 % crystal violet for 20 min. The non-migrated cells in the upper chambers were eliminated using a cotton swab. Photographs were taken of the cells in three randomly selected microscopic areas, and the number of cells that had moved was measured.

Flow cytometry analysis

Collecting mGSTc01 and Cajal cells, wash twice with PBS, then block with an CD16/32 antibody (Biolegend) for 10 min, followed by incubation with a c-kit antibody (Biolegend) conjugated to a fluorophore for 1 hour. Then, the cells were acquired using a FACS Canto II flow cytometer (BD Biosciences, CA, USA) and the data were analyzed using FlowJo VX software (FlowJo LLC, OR).

Quantitative real-time PCR

The extraction of total RNA was performed using an E.Z.N.A. Total RNA Kit I (Omega Bio-Tek, USA) following the instructions provided by the manufacturer. The entire RNA was subjected to reverse transcription using a Transcriptor First Strand cDNA Synthesis Kit (Bimake, Houston, TX, USA). The PCR system was created by combining primers, SYBR Green I Master Mix (Bimake), and cDNA templates. The qPCR experiment was conducted using a Roche LightCycler 480 real-time PCR apparatus. The thermal cycling conditions consisted of 45 cycles at 95 °C for 10 s, followed by 60 °C for 20 s, and finally 72 °C for 20 s. The mRNA expression levels of the target genes were standardized using a housekeeping gene, ACTB, and then compared to the control group. In summary, the $2^{-\Delta\Delta CT}$ technique was used to determine the relative quantities of mRNA. The primers were designed and synthesized by Sangon Biotech (Shanghai, China) and the sequences are listed in Table 2.

Cell viability assay

The viability of mGSTc01 and Cajal cells were measured by the Cell Counting Kit-8 (CCK8) assay (TargetMol). Briefly, mGSTc01 and Cajal cells (5×10^3 cells/well) were seeded in 96-well plates and cultured overnight. Then, the cells were treated with different concentrations of Imatinib (Glpbio). The medium was discarded, and the cells were incubated with CCK8 at 37 °C for 2 h. Formazan was dissolved in DMSO and optical density was read in a microplate reader with a wavelength of 450 nm.

DNA extraction and library construction

Genomic DNA was extracted from mGSTc01 and Cajal cells using Multi Sample DNA Kit (Cratbiotch). The Nanodrop spectrophotometer (Thermo Fisher Scientific, Inc., Wilmington, DE) was used to measure the amount of DNA and assess its quality. Additionally, DNA integrity was evaluated using 1 % agarose electrophoresis. Mouse genomic DNA samples were obtained using the Agilent SureSelect Human All Exon v8 library (Agilent Technologies, USA) according to the instructions provided by the manufacturer. Briefly, the genomic DNA was sheared into short fragments using the kit's enzyme. The fragmented deoxyribonucleic acid (DNA) was cleansed and processed using the reagents included in the kit, following the specified methodology. Agilent

Table 2
List of primer sequences for the qPCR assay.

Gene	Forward primer	Reverse primer
c-kit	AATATCCTCCTCACTCACGGG	TCACGGAATGGTCCACCACCA
LAMB1	CAGAATGGAAATCCGAGAGAA	CAGTCTCAGAATCACAAGGATT
MMP9	CAGCCGACTTTTGTGGTCTT	CATTTGAGTTTCCATAGTAAG
MMP2	ACCACAACCAACTACGATGATGAC	GGGCTGCCACGAGGAATAGG
CD44	CAAGTGCGAACCAGGACAGTG	CAGAGCCAGTGCCAGGAGAG
CHI3L1	TGCGGTCCTGATGCTGCTC	AGGTTGGATGGCGTCTGGTAAG
Col1a2	ACGATGTTGAACTTGTTGCTGAGG	AAGGAACGGCAGGCGAGATG
Col3a1	TTCTCCTGGTGCTGCTGGTC	ATGTGGTCCAACTGGTCCTCTG
Col4a2	CCTGCCACTACTTCGCTAACAAG	GCTGATGTGCGTGCGGATG

adapters were attached to the polished ends, and the libraries were amplified using polymerase chain reaction (PCR). The amplified libraries underwent hybridization with the bespoke probes. The DNA fragments that were attached to the probes were cleansed and extracted using the buffer included in the kit. Subsequently, the libraries underwent sequencing using the Illumina sequencing technology (NovaSeq 6000, Illumina, Inc., San Diego, CA), resulting in the generation of 150 bp paired-end reads. The whole exome sequencing and analysis were conducted by OE Biotech Co., Ltd. (Shanghai, China).

Sanger sequencing analysis

Quantify the sample and primers. Add the quantified template and primers, along with BigDye reagents, to the reaction system and complete the sequencing reaction on a PCR machine. Utilize a 3730xl DNA Analyzer (US, Applied Biosystems) to read the base sequence of the measured sample.

RNA sequencing analysis

The isolation and purification of total RNA was performed using TRIzol reagent (Cat. 15,596,018, Invitrogen, Carlsbad, CA, USA) according to the manufacturer's instructions. The concentration and integrity of the RNA were assessed using the NanoDrop ND-1000 (NanoDrop, Wilmington, DE, USA) and Bioanalyzer 2100 (Agilent, CA, USA). Next, poly (A) RNA was isolated from 1 μg total RNA using Dynabeads Oligo (dT) 25–61,005 (Thermo Fisher, CA, USA) via two rounds of purification. Next, the poly(A) RNA was fragmented using the Magnesium RNA Fragmentation Module (Cat. e6150, NEB, NY, USA) at a temperature of 94 °C for a duration of 5–7 min. The fragmented RNA fragments were reverse transcribed into cDNA using SuperScript™ II Reverse Transcriptase (Cat.1896649, Invitrogen, USA) and sequenced using illumina Novaseq™ 6000 (LC-Bio Technology CO., Ltd., Hangzhou, China). Subsequently, the expression levels of all transcripts were assessed using StringTie and edgeR. The mRNAs and genes that showed significant differences in expression were selected using the edgeR. Specifically, those with a log2 (fold change) >1 or less than −1, and a statistical significance (P value) of <0.05 were chosen. The volcano plot displayed the distributions of log2 fold change and P values for the genes that were expressed differently. The GO terms (http://www.geneontology. org) of these differentially expressed genes were annotated.

Statistical analysis

All in vitro experiments were conducted with at least three independent replicates. All in vitro studies were performed using a minimum of three independent repetitions. The data were expressed as the mean ± standard error of the mean (SEM) values. Statistical analyses were conducted using GraphPad Prism 7.0 software (GraphPad Software, Inc., San Diego, CA, USA). The significance of differences was evaluated using an unpaired two-tailed *t*-test for two groups or a one-way analysis of variance (ANOVA). A p-value of <0.05 indicates a statistically significant difference.

Result

Construction of mouse gastrointestinal stromal tumor

We developed a mouse model for GIST by using a suture impregnated with 3- methylcholanthrene into the muscularis layer of the stomach's greater curvature (Fig. 1A). Three months later, we observed that gastric tissues in mice with sutures had developed tumors, in contrast to the normal tissues (Fig. 1B). HE staining found that the mouse tumors involved the intrinsic muscle layer of the stomach, exhibiting a spindle-shaped appearance under the microscope, consistent with the primary morphological characteristics and growth pattern of GIST (Fig. 1C) [17]. IHC revealed that the GIST-associated markers, c-kit and DOG-1, were positive. Additionally, the expression of α-SMA, S-100, and SDHB was weakly positive, while Desmin expression was negative (Fig. 1D).

The extract and characteristics of the mouse GIST monoclonal cell line

To further obtain a mouse GIST monoclonal cell line, a portion of the tumor tissue was utilized for the isolation of primary tumor cells as follows (Fig. 2A). Then, we compared the extracted primary cells, gastrointestinal stromal tumors from mice, named mGSTc01, with the Cajal cells from the same mouse gastric mesenchymal tissue under a microscope. Upon microscopic examination, the mGSTc01 cells exhibited a more slender morphology compared to the Cajal cells (Fig. 2B). To confirm that the isolated primary cells possess the characteristics of mesenchymal tumors, we first performed flow cytometry analysis on mGSTc01 cells and Cajal cells using c-kit antibodies. Compared to the positive expression of c-kit in Cajal cells, mGSTc01 cells also expressed c-kit positively (Fig. 2C). Additionally, cell immunofluorescence revealed the expression of GIST-related biomarkers in mGSTc01; both c-kit and Dog-1 were positive (Fig. 2D and E). Additionally, cell immunofluorescence revealed the expression of GIST-related biomarkers in mGSTc01; both c-kit and Dog-1 were positive (Fig. 2D and E).

Additionally, we conducted Short Tandem Repeats (STR) testing to verify the mGSTc01 cell line's origin and to ensure there was no cross-contamination. The STR analysis confirmed that the cell line was of mouse origin and showed no signs of cross-contamination. Furthermore, no identical cell line to mGSTc01 was identified in the cell bank database, Cellosaurus (Table 3).

Whole exome sequencing (WES) analysis of mGSTc01

As gastrointestinal stromal cells carry mutations in multiple genes, we performed whole exome sequencing on the mGSTc01 cell line. The mutations in Lamb1, MMP9 and c-kit related bases were detected in mGSTc01 cells by Sanger sequencing (Fig. 3A). And the results of Copy number variation (CNV) revealed the Genome-wide CNV distribution of mGSTc01 and Cajal cells (Fig. 3B). Furthermore, the insertion and deletion (Indel) of mGSTc01 were primarily associated with cell adhesion and cell junction. And single nucleotide polymorphisms (SNP) mainly enriched on transcription regulatory region DNA binding (Fig. 3C).

Functional analysis of mGSTc01

To illustrate the functional characteristics of mGSTc01 cells, we conducted RNA sequencing (RNA-seq) analysis on mGSTc01 and Cajal cells. The volcano plot revealed thousands of differentially expressed genes, including 3456 upregulated genes and 5831 downregulated genes (Fig. 4A). Gene Ontology (GO) enrichment analysis showed that the most significantly expressed genes in samples from mGSTc01were associated with several GO terms related to the cell adhesion (Fig. 4B). Kyoto Encyclopedia of Genes and Genomes (KEGG) enrichment analysis of the RNA-seq results showed that mGSTc01 were associated with the categories 'ECM-receptor interaction' and 'Focal adhesion' (Fig. 4C and D). Expression levels of six genes—MMP2, CD44, CHI3L1, COL1A2, COL3A1, and COL4A2—were markedly higher in mGSTc01 cells than in Cajal cells (Fig. 4E).

Malignant behaviors and aggressive phenotypes in mGSTc01

In Transwell and cell adhesion assays, we found that mGSTc01 cell lines exhibited stronger migration and adhesion abilities (Fig. 5A and 5B). Subsequent wound healing experiments also yielded the same result, demonstrating that mGSTc01 cells had a greater migratory ability than Cajal cells at various time points (Fig. 5C). Furthermore, cell proliferation experiments using EdU staining showed that the number of

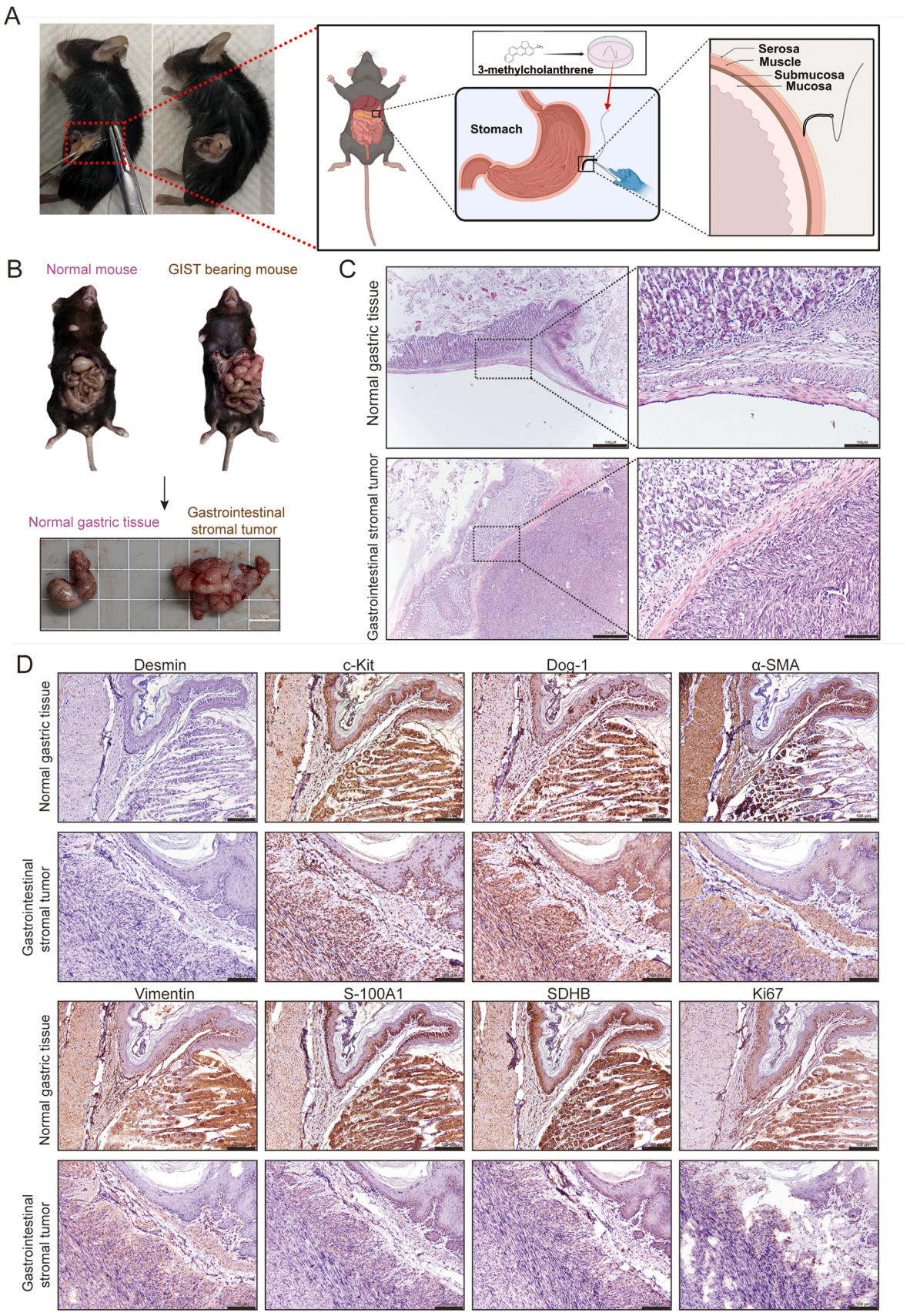

Fig. 1. Construction of Mouse Gastrointestinal Stromal Tumor. A) The process of constructing Gastrointestinal Stromal Tumor (GIST). B) The formation of GIST and the overall view of tumor C) Hematoxylin-eosin (H&E) staining of normal gastric tissue and GIST. D) Immunohistochemical (IHC) of normal gastric tissue and GIST. Scale bar: 100 μm.

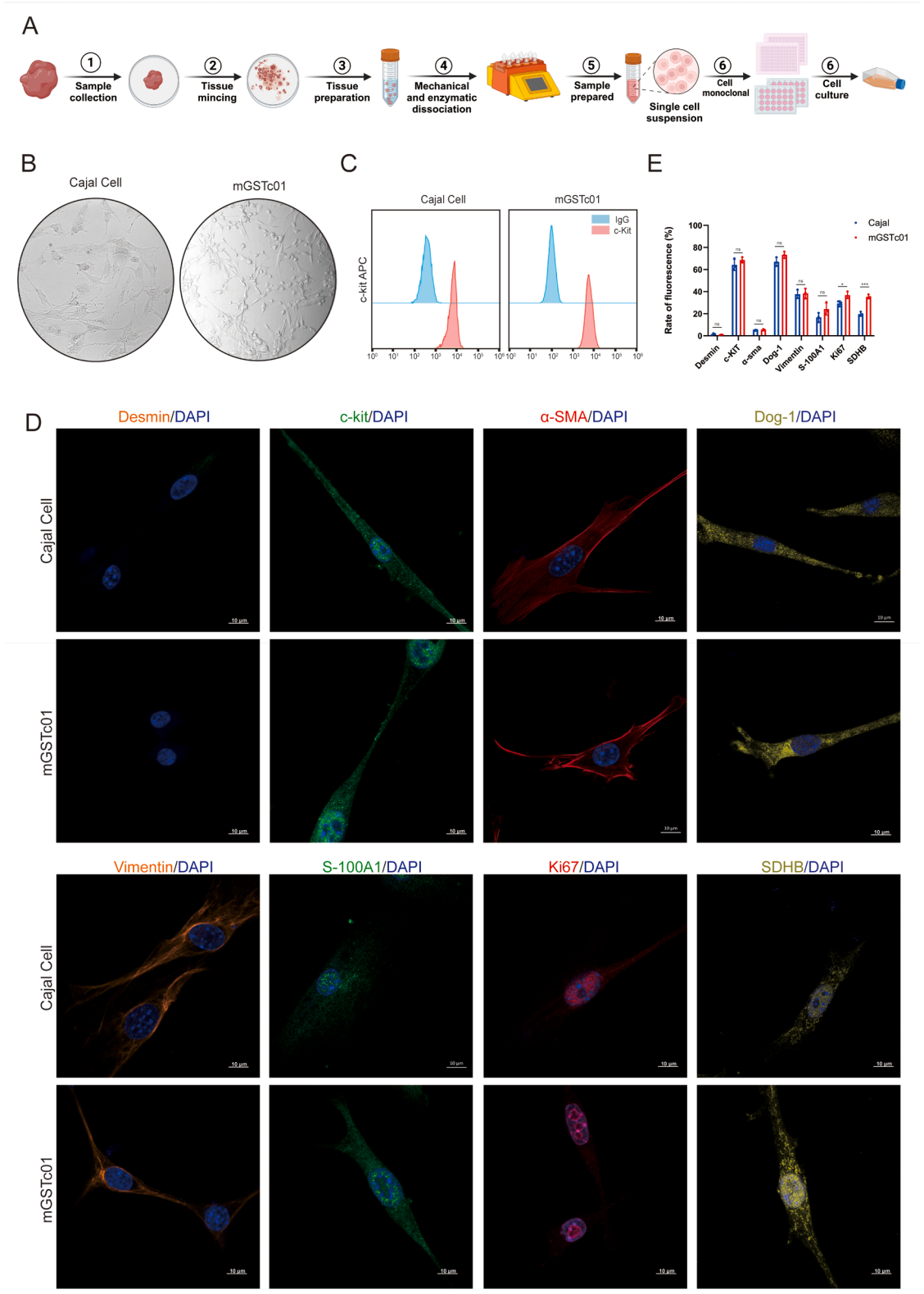

Fig. 2. The extract and characteristics of the Mouse GIST monoclonal cell line. A) The process of mGSTc01 cell line extraction and construction. B) Morphology of Cajal cells and mGSTc01 cells under light microscopy C) Flow cytometry results of Cajal cells and mGSTc01. D) Cell immunofluorescence analysis of Cajal cells and mGSTc01. Scale bar: 100 μm. E) Quantitative analysis (fluorescence intensity of positive cells) of Cajal cells and mGSTc01. * $P < 0.05$; *** $P < 0.001$.

EdU-positive cells in mGSTc01 was higher than in Cajal cells (Fig. 5D).

Exploring the therapeutic potential of mGSTc01 cells in clinical applications

We successfully established subcutaneous xenografted tumors in

Table 3
STR testing results for mGSTc01.

Marker	18–3	4–2	6–7	19–2	1–2	7–1	8–7	1–1	3–2	2–1	15–3	6–4	13–1	11–2	TH01	D5S818	17–2	12–1	5–5	X-1
Allele 1	16	20.3	17	13	19	27.2	16	16	14	15	22.3	18	17.1	16			16	17	18	27
Allele 2			18																	
Allele 3																				
Allele 4																				

immunocompetent mice (Fig. 6A), and the tumor characteristics were found to be consistent with the features of the chemically induced GIST, as evidenced by positive immunohistochemical staining for c-kit and Dog-1 (Fig. 6B). Additionally, the sensitivity of mGSTc01 cells to imatinib was assessed. Imatinib significantly decreased the viability of mGSTc01 cells in a concentration-dependent manner (Fig. 6C). Similarly, the C57BL/6 J mice bearing mGSTc01 xenografts were also sensitive for imatinib (Fig. 6D).

Discussion

Here, we report the generation of a murine GIST model through a chemical drug-induced approach. After identifying the tumor as GIST by H&E and IHC, we isolated the primary cell line, cultured it as monoclonal cells, and then phenotypically characterized and compared them to Cajal cells. Transcriptome sequencing analysis and experimental validation confirmed the phenotype of mGSTc01, which also showed a notable sensitivity to Imatinib. Additionally, using a subcutaneous tumor model, we demonstrated that these GIST cells are capable of growing within immunocompetent mice, providing a promising cellular platform for advancing immunotherapeutic strategies against GIST.

Our research has found that GST cells exhibit robust capabilities for invasion and proliferation. Analysis of our transcriptomic data reveals that mGSTc01 cells are predominantly enriched in pathways associated with cell adhesion (Fig. 4B-D). Exon sequencing also suggests a significant enrichment of extracellular matrix (ECM) related protein molecules within GIST cells, which was consistent with previous study concerning the human GIST [18]. ECM is closely related to the growth of solid tumors and fibrosis, especially the collagenase family [19]. Moreover, that heightened tissue rigidity activates intracellular signaling pathways like Rho-ROCK-MLC, enhancing integrin expression, focal adhesion, cell contractility, and EMT markers, thereby boosting cancer cells' metastatic capacity [20]. SPARCL1, a type of extracellular matrix glycoprotein, can regulate the adhesion, migration, and proliferation of GIST cells, influencing tumor growth [21]. Furthermore, our research also discovered nonsynonymous mutation in ECM-related genes Lamb1 and MMP9 may confer upon GST cells the ability to exhibit robust proliferation, adhesion, and invasiveness (Fig. 3A). Previous studies have reported that miR-374b can augment the invasive capabilities of GIST by upregulating the expression of MMP2 and MMP9 [22], suggesting that GST cells exhibit a heightened invasive phenotype.

Additionally, compared to current genetically engineered GIST mouse models [15] or human-derived cell lines such as GIST882 [23], GIST-T1 [23,24], as well as mouse S2 cell lines [15], our chemical drug approach offers a more rapid and cost-effective means of generating tumors with similar pathological characteristics. This advancement is significant because it provides researchers with a more accessible model to study the disease's progression and response to therapeutic interventions. Meanwhile, our chemical induction method allows for the rapid generation of GIST tumors, including the mGSTc01 cell line, facilitating high-throughput screening of potential drugs and therapeutic strategies [25]. Contrasted with the mouse GIST cell line extracted from gene-edited mice [15], the mGSTc01 cell line, characterized by its ease of acquisition and monoclonal nature, exhibits enhanced genetic stability. This trait is particularly advantageous for the consistency and reliability of research outcomes in subsequent studies. The establishment of the PDX model, which involves transplanting tumor tissues or primary cells into immunodeficient mice, maintains genetic characteristics to a significant degree. However, because tumors implanted in immunodeficient mice lack an immune system, the PDX model is not well-suited for research into immunotherapy. In contrast, our ability to generate tumors with mGSTc01 cells in immunocompetent mice offers advantages for future immunotherapy research on GIST (Fig. 6B). Additionally, the therapeutic application of Imatinib in these mice provides a foundational framework for advancing immunotherapeutic research.

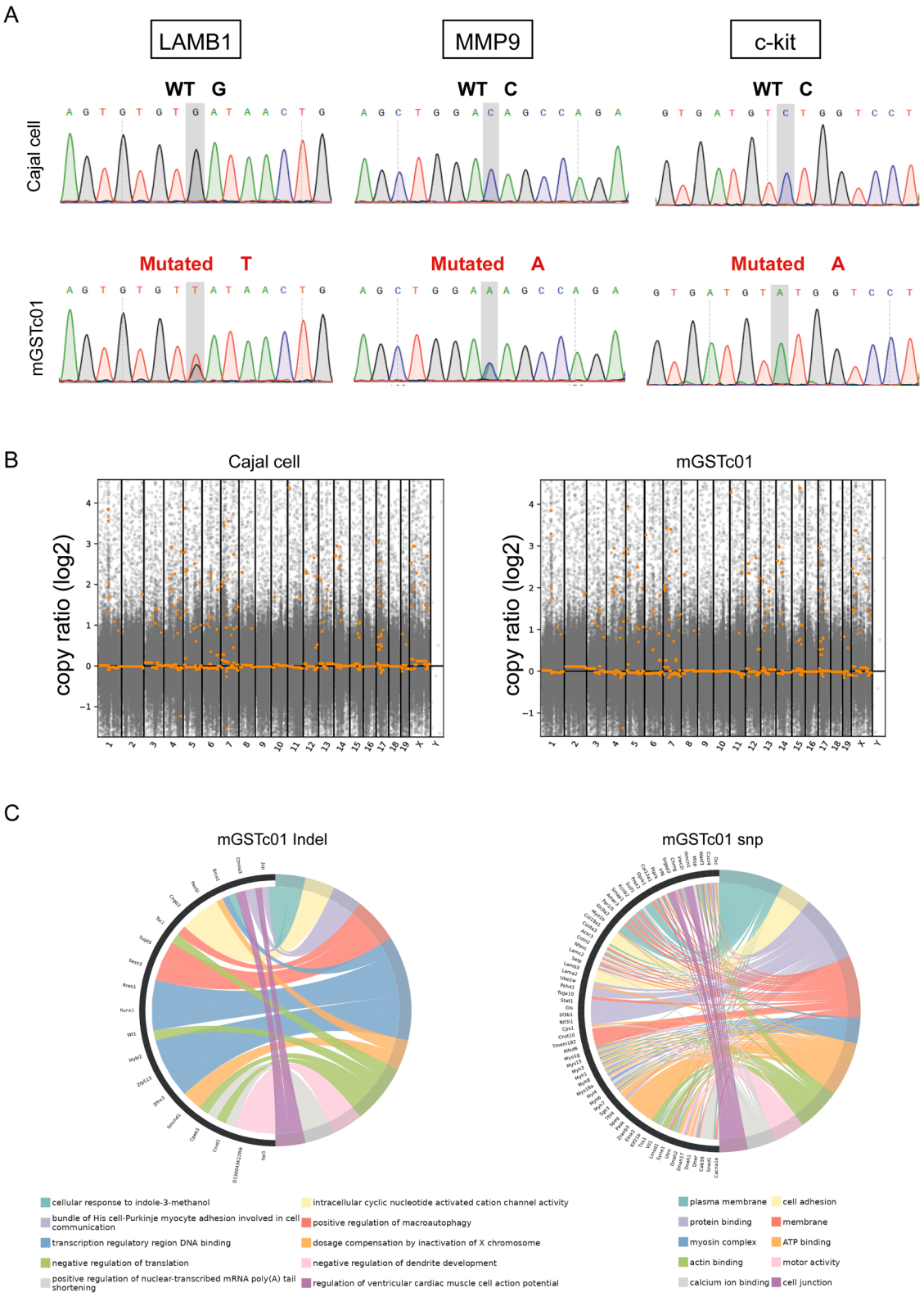

Fig. 3. Whole exome sequencing (WES) analysis of mGSTc01. A) Sanger sequencing detected identical LAMB1, MMP9 and c-kit mutations in Cajal and mGSTc01. B) Display the distribution of whole-genome copy number variations (CNVs) of Cajal and mGSTc01 using the copy ratio (log2). The horizontal axis represents the chromosome number, and the vertical axis represents the copy ratio (log2). C) The Chord Diagram showed the Single Nucleotide Polymorphisms (SNP) and Insertion and Deletion (InDel) of mGSTc01.

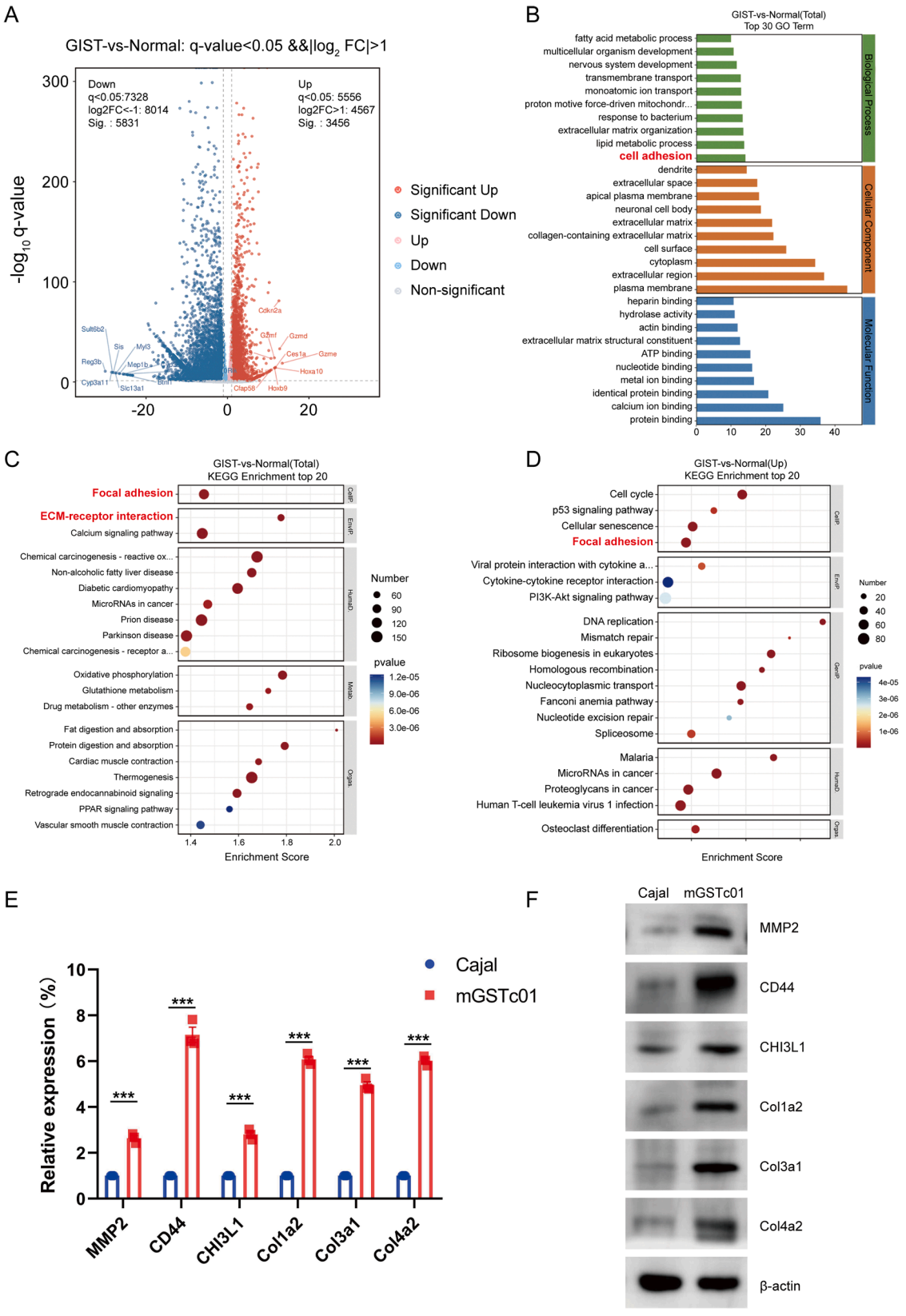

Fig. 4. Functional Analysis of mGSTc01. A) Volcano plot of differential genes between Cajal cell and mGSTc01 B) Gene Ontology (GO) Enrichment Analysis between Cajal cell and mGSTc01. C) Kyoto Encyclopedia of Genes and Genomes (KEGG) enrichment analysis of Cajal and mGSTc01. D) The KEGG show the top 20 pathway enrichment of mGSTc01 compared with Cajal. E) The relative mRNA expression of ECM. F) The relative protein expression levels of ECM. *** $P < 0.001$.

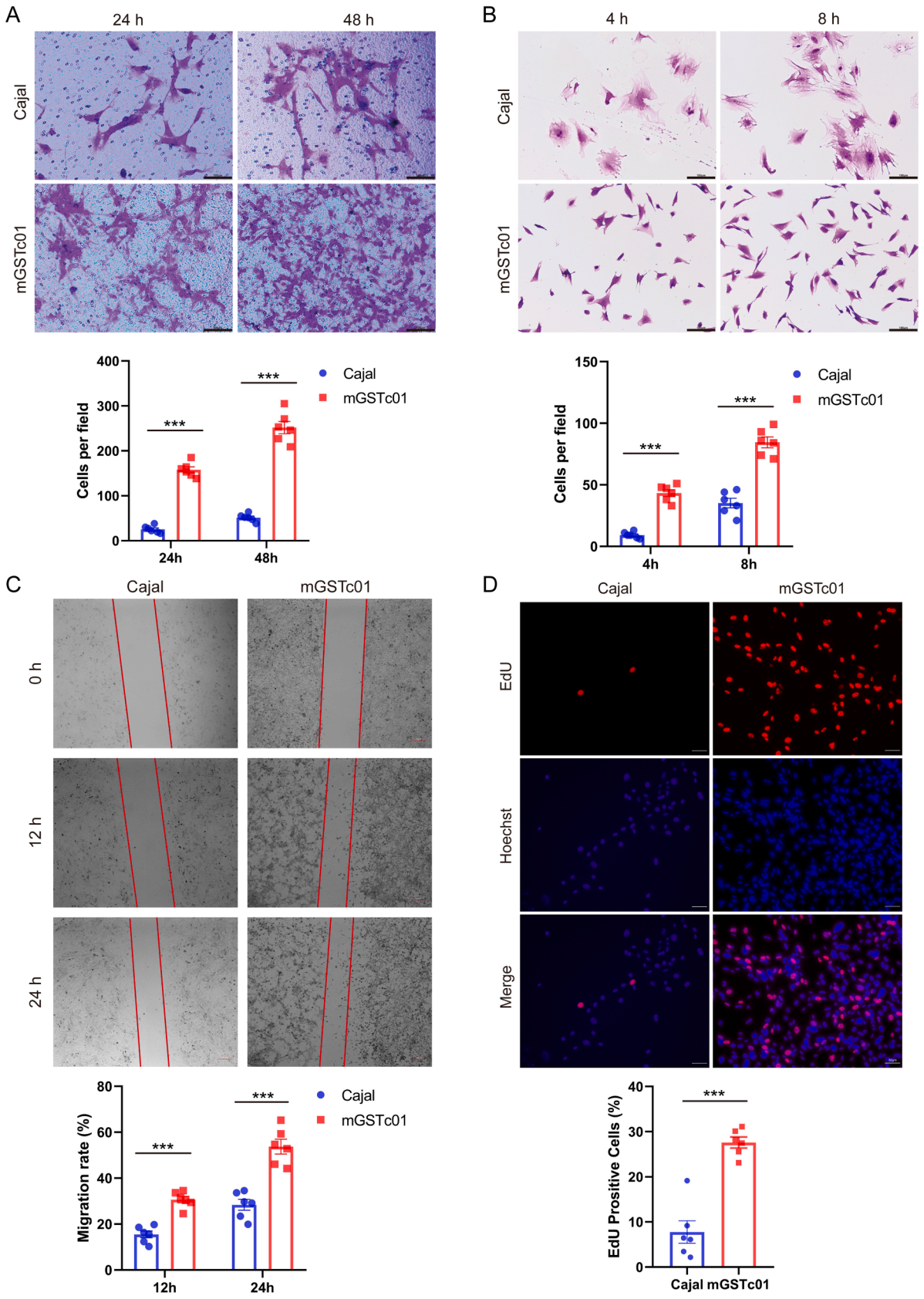

Fig. 5. The phenotype of mGSTc01 cells. A) mGSTc01 cells and Cajal cells were observed for 24 and 48 h. Representative image of migrated cells. Scale bar: 100 μm. Quantification of the number of migrated cells were shown. B) Representative images of mGSTc01 and Cajal cells adhered to fibronectin and quantification of the number of mGSTc01 and Cajal cell adhered to fibronectin ($n = 6$). C) Representative images and quantitative analysis of mGSTc01 and Cajal cells migration based on wound healing assay. D) EdU assay in mGSTc01 and Cajal cells was performed to measure the proliferation ability. Scale bar: 50 μm. *** $P < 0.001$.

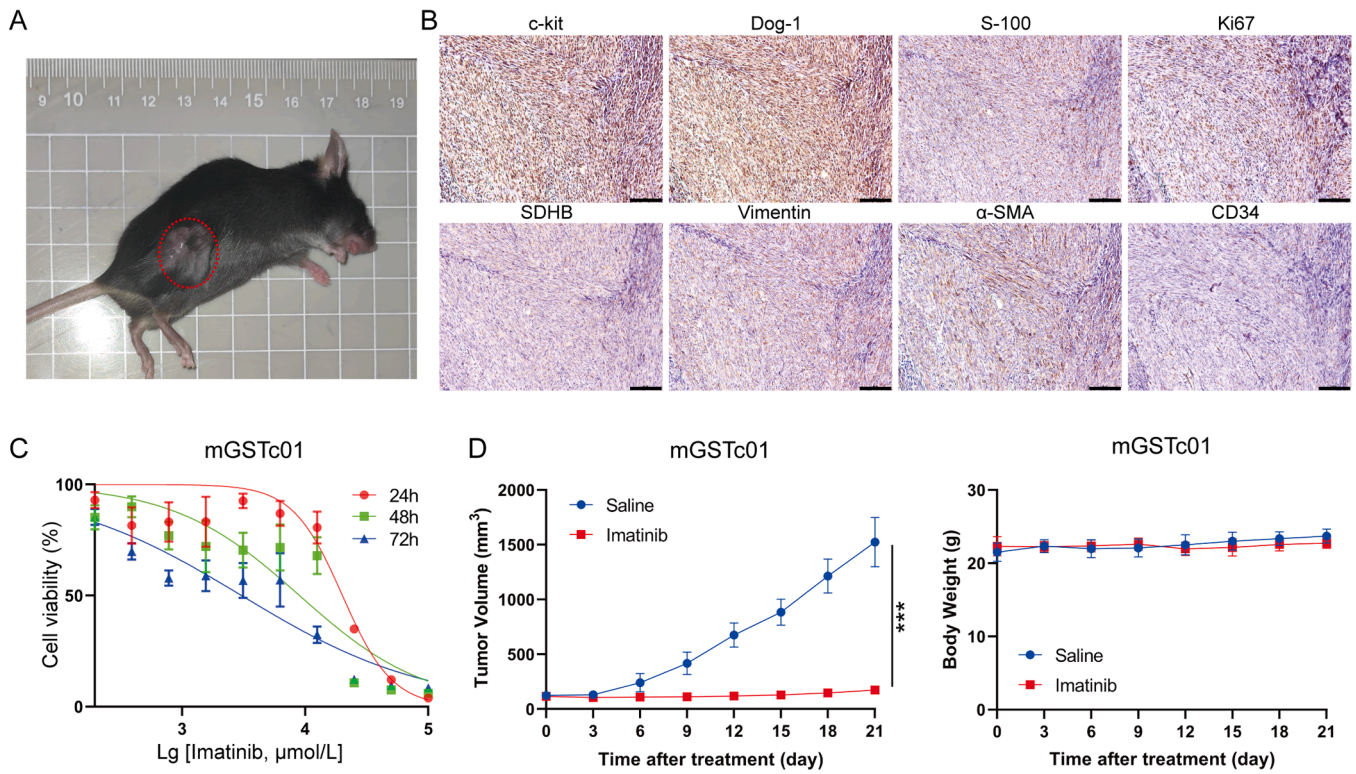

Fig. 6. The application of mGSTc01 cells. A) Construction of Subcutaneous Tumors with mGSTc01 Cells. B) IHC staining of GIST marker in mGSTc01 xenograft tumors. Scale bar: 100 μm for IHC images. C) mGSTc01 cells were treated with various concentrations of imatinib for 24, 48, and 72 h. Cell viability was detected by CCK-8 assay. D) C57BL/6 J mice bearing mGSTc01 tumors were treated with Saline (0.9 % NaCl solution containing 1 % DMSO) or imatinib (10 mg/kg, i.p.) every three days. The tumor volumes of tumor-bearing mice were measured every three days. (D, left). The weights of mice were shown (D, right). *** $P < 0.001$.

Currently, immunotherapy is becoming a promising cancer therapy, heralding a personalized approach to treatment. The dense infiltration of immune cells, including T cells [26,27], tumor-associated macrophages (TAMs) [28], and NK cells [29], etc., within GIST tumors suggests a profound potential for immunotherapeutic intervention, presenting a compelling opportunity for targeted cancer treatment. A multitude of clinical studies have been initiated to explore this therapeutic avenue. Despite the majority of these trials not meeting their endpoints, the lack of success does not negate the potential for GIST to respond favorably to immunotherapeutic strategies [30–33]. Nevertheless, emerging research indicates that GIST patients characterized by PDGFRA D842V mutations, a KIT-wild type (WT) genotype, or elevated expression levels of PD-L1 may exhibit a heightened response to immune checkpoint inhibitors (ICIs). This subset of patients should, therefore, be considered for preferential selection [34,35]. Moreover, research found the combination of imatinib and ipilimumab was synergistic and significantly reduced tumor size compared to either treatment alone in KIT mutant GIST mouse models [36]. In our researches, we also constructed in vivo GIST model in C57BL/6 J mouse using mGSTc01 cell, which is more convenient and quicker to conduct immunotherapy research on GIST. Therefore, for the future treatment of GIST, especially in immunotherapy, we have superior cellular and animal models available for research. This further provides a research foundation for the treatment of GIST.

In conclusion, we have developed a mouse model of GIST using chemical induction methods and successfully isolated and cultured a new monoclonal cell line, named mGSTc01. This cell line's fidelity to the molecular characteristics of human disease, coupled with its potential for studying both targeted therapies and immunotherapies, makes it a powerful tool for enhancing our understanding of GIST pathogenesis and treatment. Future research will leverage the unique features of this cell model to gain new insights into GIST biology and to discover innovative therapeutic strategies

Data availability

Additional data or resources related to this article are available upon reasonable request from the corresponding authors.

CRediT authorship contribution statement

Zhan Zhao: Writing – original draft, Visualization, Resources, Methodology, Conceptualization. **Shenghui Qiu:** Validation, Formal analysis, Data curation. **Xiangwei Zhang:** Software, Resources, Methodology, Data curation. **Shijin Liu:** Software, Methodology. **Lu Wang:** Validation, Software. **Hanyang Guan:** Methodology, Investigation. **Jiashuai He:** Methodology, Investigation, Formal analysis. **Yangzhi Hu:** Methodology, Formal analysis. **Xiaobo Li:** Methodology, Investigation, Formal analysis. **Simin Luo:** Project administration, Funding acquisition. **Zuyang Chen:** Methodology, Investigation. **Tianmu Mo:** Methodology. **Yiran Zhang:** Visualization, Validation, Resources. **Xiaoxu Zhao:** Validation, Supervision, Software. **Yunlong Pan:** Writing – review & editing, Investigation, Conceptualization. **Hui Ding:** Writing – review & editing, Project administration, Funding acquisition. **Jie Cao:** Writing – review & editing, Project administration, Investigation, Funding acquisition. **Jinghua Pan:** Writing – review & editing, Writing – original draft, Resources, Project administration, Methodology, Funding acquisition.

Declaration of competing interest

The authors declare that they have no known competing financial interests or personal relationships that could have appeared to influence the work reported in this paper.

Acknowledgements

This research was supported by the National Natural Science Foundation of China (82204436, 82173236), Natural Science Foundation of Guangdong Province (2024A1515030010, 2022A1515011695), Guangzhou Science and Technology Plan City-School Joint Funding Project (202201020084), Funding by Science and Technology Projects in Guangzhou (202201020566, 2024A03J0825), Guangzhou High-level Key Clinical Specialty Construction Project (No.9), Guangzhou Science and Technology Planning Project (202206080008).

References

[1] N.C. Campanella, A.T. de Oliveira, C. Scapulatempo-Neto, D.P. Guimarães, R. M. Reis, Biomarkers and novel therapeutic targets in gastrointestinal stromal tumors (GISTs), Recent Pat Anticancer Drug. Discov. 8 (2013) 288–297, https://doi.org/10.2174/1574892811308999003O.

[2] K. Søreide, O.M. Sandvik, J.A. Søreide, V. Giljaca, A. Jureckova, V.R. Bulusu, Global epidemiology of gastrointestinal stromal tumours (GIST): a systematic review of population-based cohort studies, Cancer Epidemiol. 40 (2016) 39–46, https://doi.org/10.1016/j.canep.2015.10.031.

[3] P.G. Casali, J.Y. Blay, N. Abecassis, J. Bajpai, S. Bauer, R. Biagini, S. Bielack, S. Bonvalot, I. Boukovinas, J. Bovee, K. Boye, T. Brodowicz, A. Buonadonna, E. De Álava, A.P. Dei Tos, X.G. Del Muro, A. Dufresne, M. Eriksson, A. Fedenko, V. Ferraresi, A. Ferrari, A.M. Frezza, S. Gasperoni, H. Gelderblom, F. Gouin, G. Grignani, R. Haas, A.B. Hassan, N. Hindi, P. Hohenberger, H. Joensuu, R. L. Jones, C. Jungels, P. Jutte, B. Kasper, A. Kawai, K. Kopeckova, D.A. Krákorová, A. Le Cesne, F. Le Grange, E. Legius, A. Leithner, A. Lopez-Pousa, J. Martin-Broto, O. Merimsky, C. Messiou, A.B. Miah, O. Mir, M. Montemurro, C. Morosi, E. Palmerini, M.A. Pantaleo, R. Piana, S. Piperno-Neumann, P. Reichardt, P. Rutkowski, A.A. Safwat, C. Sangalli, M. Sbaraglia, S. Scheipl, P. Schöffski, S. Sleijfer, D. Strauss, S.J. Strauss, K.S. Hall, A. Trama, M. Unk, M.A.J. van de Sande, W.T.A. van der Graaf, W.J. van Houdt, T. Frebourg, A. Gronchi, S. Stacchiotti, Gastrointestinal stromal tumours: ESMO-EURACAN-GENTURIS Clinical Practice guidelines for diagnosis, treatment and follow-up, Ann. Oncol. 33 (2022) 20–33, https://doi.org/10.1016/j.annonc.2021.09.005.

[4] A. Poveda, X. García Del Muro, J.A. López-Guerrero, R. Cubedo, V. Martínez, I. Romero, C. Serrano, C. Valverde, J. Martín-Broto, GEIS guidelines for gastrointestinal sarcomas (GIST), Cancer Treat. Rev. 55 (2017) 107–119, https://doi.org/10.1016/j.ctrv.2016.11.011.

[5] J. Zhang, K. Chen, Y. Tang, X. Luan, X. Zheng, X. Lu, J. Mao, L. Hu, S. Zhang, X. Zhang, W. Chen, LncRNA-HOTAIR activates autophagy and promotes the imatinib resistance of gastrointestinal stromal tumor cells through a mechanism involving the miR-130a/ATG2B pathway, Cell Death. Dis. 12 (2021) 367, https://doi.org/10.1038/s41419-021-03650-7.

[6] N. Kang, H. Gu, Y. Ni, X. Wei, S. Zheng, Prognostic and clinicopathological significance of the Prognostic Nutritional Index in patients with gastrointestinal stromal tumours undergoing surgery: a meta-analysis, BMJ Open 12 (2022) e064577, https://doi.org/10.1136/bmjopen-2022-064577.

[7] M. Miettinen, J. Lasota, Gastrointestinal stromal tumors: pathology and prognosis at different sites, Semin. Diagn. Pathol. 23 (2006) 70–83, https://doi.org/10.1053/j.semdp.2006.09.001.

[8] S. Hirota, K. Isozaki, Y. Moriyama, K. Hashimoto, T. Nishida, S. Ishiguro, K. Kawano, M. Hanada, A. Kurata, M. Takeda, G. Muhammad Tunio, Y. Matsuzawa, Y. Kanakura, Y. Shinomura, Y. Kitamura, Gain-of-function mutations of c-kit in human gastrointestinal stromal tumors, Science 279 (1998) 577–580, https://doi.org/10.1126/science.279.5350.577.

[9] M.C. Heinrich, C.L. Corless, A. Duensing, L. McGreevey, C.J. Chen, N. Joseph, S. Singer, D.J. Griffith, A. Haley, A. Town, G.D. Demetri, C.D. Fletcher, J. A Fletcher, PDGFRA activating mutations in gastrointestinal stromal tumors, Science 299 (2003) 708–710, https://doi.org/10.1126/science.1079666.

[10] X. Guo, Y. Li, B. Wan, Y. Lv, X. Wang, G. Liu, P. Wang, ETV1 inhibition depressed M2 polarization of tumor-associated macrophage and cell process in gastrointestinal stromal tumor via down-regulating PDE3A, J. Clin. Biochem. Nutr. 72 (2023) 139–146, https://doi.org/10.3164/jcbn.22-47.

[11] X. Liu, J. Yu, Y. Li, H. Shi, X. Jiao, X. Liu, D. Guo, Z. Li, Y. Tian, F. Dai, Z. Niu, Y. Zhou, Deciphering the tumor immune microenvironment of imatinib-resistance in advanced gastrointestinal stromal tumors at single-cell resolution, Cell. Death. Dis. 15 (2024) 190, https://doi.org/10.1038/s41419-024-06571-3.

[12] G. Sommer, V. Agosti, I. Ehlers, F. Rossi, S. Corbacioglu, J. Farkas, M. Moore, K. Manova, C.R. Antonescu, P. Besmer, Gastrointestinal stromal tumors in a mouse model by targeted mutation of the Kit receptor tyrosine kinase, Proc. Natl Acad. Sci. 100 (2003) 6706–6711, https://doi.org/10.1073/pnas.1037763100.

[13] K. Iida, A.H. Abdelhamid Ahmed, A.K. Nagatsuma, T. Shibutani, S. Yasuda, M. Kitamura, C. Hattori, M. Abe, J. Hasegawa, T. Iguchi, T. Karibe, T. Nakada, K. Inaki, R. Kamei, Y. Abe, T. Nomura, J.L. Andersen, S. Santagata, M.L. Hemming, S. George, T. Doi, A. Ochiai, G.D. Demetri, T. Agatsuma, Identification and therapeutic targeting of GPR20, selectively expressed in gastrointestinal stromal tumors, with DS-6157a, a first-in-class antibody-drug conjugate, Cancer Discov. 11 (2021) 1508–1523, https://doi.org/10.1158/2159-8290.cd-20-1434.

[14] B.D. Smith, M.D. Kaufman, W.P. Lu, A. Gupta, C.B. Leary, S.C. Wise, T.J. Rutkoski, Y.M. Ahn, G. Al-Ani, S.L. Bulfer, T.M. Caldwell, L. Chun, C.L. Ensinger, M.M. Hood, A. McKinley, W.C. Patt, R. Ruiz-Soto, Y. Su, H. Telikepalli, A. Town, B.A. Turner, L. Vogeti, S. Vogeti, K. Yates, F. Janku, A.R. Abdul Razak, O. Rosen, M.C. Heinrich, D.L Flynn, Ripretinib (DCC-2618) is a switch control kinase inhibitor of a broad spectrum of oncogenic and drug-resistant KIT and PDGFRA variants, Cancer Cell 35 (2019) 738–751, https://doi.org/10.1016/j.ccell.2019.04.006, e9.

[15] M.J. Cavnar, S. Zeng, T.S. Kim, E.C. Sorenson, L.M. Ocuin, V.P. Balachandran, A. M. Seifert, J.B. Greer, R. Popow, M.H. Crawley, N.A. Cohen, B.L. Green, F. Rossi, P. Besmer, C.R. Antonescu, R.P. DeMatteo, KIT oncogene inhibition drives intratumoral macrophage M2 polarization, J. Exp. Med. 210 (2013) 2873–2886, https://doi.org/10.1084/jem.20130875.

[16] A. Capes-Davis, G. Theodosopoulos, I. Atkin, H.G. Drexler, A. Kohara, R. A. MacLeod, J.R. Masters, Y. Nakamura, Y.A. Reid, R.R. Reddel, R.I. Freshney, Check your cultures! A list of cross-contaminated or misidentified cell lines, Int. J. Cancer 127 (2010) 1–8, https://doi.org/10.1002/ijc.25242.

[17] M. Miettinen, J. Lasota, Gastrointestinal stromal tumors – definition, clinical, histological, immunohistochemical, and molecular genetic features and differential diagnosis, Virchows. Arch. 438 (2001) 1–12, https://doi.org/10.1007/s004280000338.

[18] M. Sun, Y. Tong, W. Yuan, Y. Wang, Y. Pu, W. Huang, B. Lv, C. Xu, W. Jiang, R. Luo, R. Fang, S. Tang, L. Ren, J. Wang, J. Feng, C. Sun, K. Shen, F. He, Y. Hou, C. Ding, Proteomic characterization identifies clinically relevant subgroups of gastrointestinal stromal tumors, Gastroenterology 166 (2024) 450–465, https://doi.org/10.1053/j.gastro.2023.11.284, e33.

[19] F.A. Venning, L. Wullkopf, J.T. Erler, Targeting ECM disrupts cancer progression, Front. Oncol. 5 (2015), https://doi.org/10.3389/fonc.2015.00224.

[20] C. Bonnans, J. Chou, Z. Werb, Remodelling the extracellular matrix in development and disease, Nat. Rev. Mol. Cell Biol. 15 (2014) 786–801, https://doi.org/10.1038/nrm3904.

[21] C. Shen, L. Han, B. Liu, G. Zhang, Z. Cai, X. Yin, Y. Yin, Z. Chen, B. Zhang, The KDM6A-SPARCL1 axis blocks metastasis and regulates the tumour microenvironment of gastrointestinal stromal tumours by inhibiting the nuclear translocation of p65, Br. J. Cancer 126 (2022) 1457–1469, https://doi.org/10.1038/s41416-022-01728-3.

[22] Z.-W. Long, J.-H. Wu, H. Cai, Y.-N. Wang, Y. Zhou, MiR-374b promotes proliferation and inhibits apoptosis of Human GIST cells by inhibiting PTEN through activation of the PI3K/Akt pathway, Mol. Cells 41 (2018) 532–544, https://doi.org/10.14348/molcells.2018.2211.

[23] S. Zeng, A.M. Seifert, J.Q. Zhang, M.J. Cavnar, T.S. Kim, V.P. Balachandran, J. A. Santamaria-Barria, N.A. Cohen, M.J. Beckman, B.D. Medina, F. Rossi, M. H. Crawley, J.K. Loo, J.H. Maltbaek, P. Besmer, C.R. Antonescu, R.P. DeMatteo, Wnt/β-catenin signaling contributes to tumor malignancy and is targetable in gastrointestinal stromal tumor, Mol. Cancer Ther. 16 (2017) 1954–1966, https://doi.org/10.1158/1535-7163.mct-17-0139.

[24] J.Q. Zhang, S. Zeng, G.A. Vitiello, A.M. Seifert, B.D. Medina, M.J. Beckman, J. K. Loo, J. Santamaria-Barria, J.H. Maltbaek, N.J. Param, J.A. Moral, J.N. Zhao, V. Balachandran, F. Rossi, C.R. Antonescu, R.P. DeMatteo, Macrophages and CD8+ T cells mediate the antitumor efficacy of combined CD40 ligation and imatinib therapy in gastrointestinal stromal tumors, Cancer Immunol. Res. 6 (2018) 434–447, https://doi.org/10.1158/2326-6066.cir-17-0345.

[25] Y. Liu, T. Yin, Y. Feng, M.M. Cona, G. Huang, J. Liu, S. Song, Y. Jiang, Q. Xia, J. V. Swinnen, G. Bormans, U. Himmelreich, R. Oyen, Y. Ni, Mammalian models of chemically induced primary malignancies exploitable for imaging-based preclinical theragnostic research, Quant. Imaging Med. Surg. 5 (2015) 708–729, https://doi.org/10.3978/j.issn.2223-4292.2015.06.01.

[26] H. Komita, S. Koido, K. Hayashi, S. Kan, M. Ito, Y. Kamata, M. Suzuki, S. Homma, Expression of immune checkpoint molecules of T cell immunoglobulin and mucin protein 3/galectin-9 for NK cell suppression in human gastrointestinal stromal tumors, Oncol. Rep. 34 (2015) 2099–2105, https://doi.org/10.3892/or.2015.4149.

[27] C. Zhuang, B. Ni, Z.Z. Zhang, W.Y. Zhao, L. Tu, X.L. Ma, L.X. Yang, H. Cao, M. Wang, Low distribution of TIM-3(+) cytotoxic tumor-infiltrating lymphocytes predicts poor outcomes in gastrointestinal stromal tumors, J. Immunol. Res. 2021 (2021) 6647292, https://doi.org/10.1155/2021/6647292.

[28] M. van Dongen, N.D. Savage, E.S. Jordanova, I.H. Briaire-de Bruijn, K.V. Walburg, T.H. Ottenhoff, P.C. Hogendoorn, S.H. van der Burg, H. Gelderblom, T. van Hall, Anti-inflammatory M2 type macrophages characterize metastasized and tyrosine kinase inhibitor-treated gastrointestinal stromal tumors, Int. J. Cancer 127 (2010) 899–909, https://doi.org/10.1002/ijc.25113.

[29] S. Rusakiewicz, M. Semeraro, M. Sarabi, M. Desbois, C. Locher, R. Mendez, N. Vimond, A. Concha, F. Garrido, N. Isambert, L. Chaigneau, V. Le Brun-Ly, P. Dubreuil, I. Cremer, A. Caignard, V. Poirier-Colame, K. Chaba, C. Flament, N. Halama, D. Jäger, A. Eggermont, S. Bonvalot, F. Commo, P. Terrier, P. Opolon, J.F. Emile, J.M. Coindre, G. Kroemer, N. Chaput, A. Le Cesne, J.Y. Blay, L. Zitvogel, Immune infiltrates are prognostic factors in localized gastrointestinal stromal tumors, Cancer Res. 73 (2013) 3499–3510, https://doi.org/10.1158/0008-5472.can-13-0371.

[30] A.S. Singh, J.R. Hecht, L. Rosen, Z.A. Wainberg, X. Wang, M. Douek, A. Hagopian, R. Andes, L. Sauer, S.R. Brackert, W. Chow, R. DeMatteo, F.C. Eilber, J.A. Glaspy, B. Chmielowski, A randomized Phase II study of Nivolumab monotherapy or Nivolumab combined with Ipilimumab in patients with advanced gastrointestinal stromal tumors, Clin. Cancer Res. 28 (2022) 84–94, https://doi.org/10.1158/1078-0432.ccr-21-0878.

[31] J.L. Chen, M.R. Mahoney, S. George, C.R. Antonescu, D.A. Liebner, B.A.V. Tine, M. M. Milhem, W.D. Tap, H. Streicher, G.K. Schwartz, S.P D'Angelo, A multicenter phase II study of nivolumab +/- ipilimumab for patients with metastatic sarcoma

(Alliance A091401): results of expansion cohorts, J. Clin. Oncol. 38 (2020), https://doi.org/10.1200/JCO.2020.38.15_suppl.11511, 11511-11511.

[32] B.A. Schroeder, K. Kohli, R.B. O'Malley, T.S. Kim, R.L. Jones, R.H. Pierce, S. M Pollack, Durable tumor regression in highly refractory metastatic KIT/PDGFRA wild-type GIST following treatment with nivolumab, Oncoimmunology 9 (2020) 1710064, https://doi.org/10.1080/2162402x.2019.1710064.

[33] Toulmonde M., Penel N., Adam J., Chevreau C., Blay J.-.Y., Cesne A.L., Bompas E., Piperno-Neumann S., Cousin S., Ryckewaert T., Bessede A., Ghiringhelli F., Grellety T., Pulido M., Italiano A. Combination of pembrolizumab and metronomic cyclophosphamide in patients with advanced sarcomas and GIST: a French Sarcoma Group phase II trial. J. Clin. Oncol. 2017;35:11053–11053.doi:10.1200/JCO.2017.35.15_suppl.11053.

[34] Zhao R., Song Y., Wang Y., Huang Y., Li Z., Cui Y., Yi M., Xia L., Zhuang W., Wu X., Zhou Y. PD-1/PD-L1 blockade rescue exhausted CD8+ T cells in gastrointestinal stromal tumours via the PI3K/Akt/mTOR signalling pathway. Cell Prolif. 2019;52:e12571.doi:10.1111/cpr.12571.

[35] Petitprez F., de Reyniès A., Keung E.Z., Chen T.W., Sun C.M., Calderaro J., Jeng Y. M., Hsiao L.P., Lacroix L., Bougoüin A., Moreira M., Lacroix G., Natario I., Adam J., Lucchesi C., Laizet Y.H., Toulmonde M., Burgess M.A., Bolejack V., Reinke D., Wani K.M., Wang W.L., Lazar A.J., Roland C.L., Wargo J.A., Italiano A., Sautès-Fridman C., Tawbi H.A., Fridman W.H. B cells are associated with survival and immunotherapy response in sarcoma. Nature 2020;577:556–560.doi:10.1038/s41586-019-1906-8.

[36] Balachandran V.P., Cavnar M.J., Zeng S., Bamboat Z.M., Ocuin L.M., Obaid H., Sorenson E.C., Popow R., Ariyan C., Rossi F., Besmer P., Guo T., Antonescu C.R., Taguchi T., Yuan J., Wolchok J.D., Allison J.P., DeMatteo R.P. Imatinib potentiates antitumor T cell responses in gastrointestinal stromal tumor through the inhibition of ido. Nat. Med. 2011;17:1094–100.doi:10.1038/nm.2438.